NRC Research Press

NOTE

An analysis of spotting distances during the 2017 fire season in the Northern Rockies, USA

Wesley G. Page, Natalie S. Wagenbrenner, Bret W. Butler, and David L. Blunck

Abstract: The wildfires that burned in the Northern Rockies region of the USA during the 2017 fire season provided an opportunity to evaluate the suitability of using broadscale and temporally limited infrared data on hot spot locations to determine the influence of several environmental variables on spotting distance. Specifically, correlations between the maximum observed spot fire distance for each unique combination of fire and day and geo-referenced environmental data on wind speed, vegetation, and terrain, along with specific fire characteristics (size, fire perimeter shape, and growth), were assessed. The data were also utilized to evaluate a popular theoretical model developed by Albini (1979) for predicting the maximum spotting distance for single and group tree torching. The results suggested a significant positive correlation between the maximum observed spot fire distance and an interaction between fire growth and wind speed. Significant negative correlations between maximum spotting distance and fire perimeter shape, canopy height, and terrain steepness were also discovered. The evaluation of Albini's (1979) model suggested that selecting a high estimate of potential wind speed was important to minimize the likelihood of underpredicting maximum spotting distance.

Key words: fire behaviour, firebrand, maximum spot fire distance, torching, torching trees.

Résumé : Les feux de forêt survenus dans la région des Rocheuses du nord aux États-Unis durant la saison des feux de 2017 ont fourni une occasion pour évaluer la pertinence d'utiliser des données infrarouges à grande échelle et limité dans le temps sur la localisation des points chauds pour déterminer l'influence de plusieurs variables environnementales sur la distance de détection. Spécifiquement, pour chaque combinaison unique de feu et de jour, les relations entre la distance maximum observée d'un feu disséminé et des données environnementales géoréférencées sur la vitesse du vent, la végétation et le terrain, ainsi que des caractéristiques spécifiques du feu (taille, forme du périmètre de feu et progression) ont été évaluées. Les données ont aussi été utilisées pour évaluer un modèle théorique populaire élaboré par Albini (1979) pour prédire la distance maximum de détection dans le cas de la flambée en chandelle d'un seul ou d'un groupe d'arbres. Les résultats indiquent qu'il y a une relation positive significative entre la distance maximum de détection d'un point chaud et une interaction entre la progression du feu et la vitesse du vent. Des relations négatives significatives entre la distance maximum de détection et la forme du périmètre de feu, la hauteur du couvert forestier et l'inclinaison du terrain ont aussi été observées. L'évaluation du modèle d'Albini (1979) indique que le choix d'une estimation élevée de la vitesse potentielle du vent est important afin de minimiser la probabilité de sous-estimer la distance maximum de détection. [Traduit par la Rédaction]

Mots-clés : comportement du feu, tison, distance maximum d'un feu disséminé, flambée en chandelle, flambée en chandelle des arbres.

Introduction

The wildfires that burned within the Northern Rockies region of the USA during the 2017 fire season were some of the largest and most expensive to manage in recent memory. In total, approximately 628 000 ha burned mostly over the three-month period of July to September, in which nine fires that each exceeded 16 000 ha in size cost about 193 million USD to manage (National Interagency Coordination Center (NICC) 2017). A wet winter and spring followed by hot, dry, and windy conditions in June and July led to above-average fire danger and fire behaviour that resisted suppression efforts (National Interagency Fire Center (NIFC) 2017). During large fire events in the USA, the National Infrared Operations program (NIROPS) is frequently requested to assist fire managers in gathering and interpreting infrared (IR) data to relay consistent and reliable information on fire position (Zajkowski et al. 2003). A team of IR technicians, interpreters, and pilots are assembled to deploy and operate aircraft-mounted IR equipment that is suited to detect small heat sources (i.e., 15–20 cm in diameter) over vast areas in a short amount of time (40.5 $km^2 \cdot min^{-1}$) (Greenfield et al. 2003). If weather conditions permit, data acquisition for multiple large fires is attempted during the night or early morning hours, with the final image resolution dependent on the altitude of the plane. The raw data are processed by IR interpreters to produce geo-corrected products that are then transmitted to fire managers.

Since the mid-1960s, a variety of mathematical models have been proposed with the purpose of predicting the distance that firebrands originating from a wildland fire can travel given vari-

Received 14 March 2018. Accepted 11 October 2018.

W.G. Page, N.S. Wagenbrenner, and B.W. Butler. USDA Forest Service, Rocky Mountain Research Station, Fire, Fuel, and Smoke Science Program, 5775 Highway 10 W, Missoula, MT 59808, USA.
D.L. Blunck. School of Mechanical, Industrial, and Manufacturing Engineering, College of Engineering, Oregon State University, 204 Rogers Hall, Corvallis, OR 97331, USA.
Corresponding author: Wesley G. Page (email: wesleygpage@fs.fed.us).

ous assumptions about firebrand size, burnout time, and the ambient environmental conditions (Pastor et al. 2003). The determination of the maximum distance that firebrands can travel and ignite new fires that are disconnected from the main fire front (i.e., spot fires) has received considerable attention, as these spot fires have the potential to be the most detrimental from the standpoint of suppression operations (Alexander 2000). Of the various proposed models, the most common operationally applied model in the USA is that of Albini (1979). Albini's (1979) model predicts the maximum distance that cylindrical particles originating from a convection column produced by a single tree or group of torching trees can travel and ignite new fires. The spotting distances produced by the model represent the theoretical farthest limit that firebrands can travel, not necessarily the distance that firebrands will travel. The model is widely applied and incorporated into several fire behavior prediction systems that are presently used operationally in the USA, including FARSITE (Finney 2004), the Wildland Fire Decision Support System (Noonan-Wright et al. 2011), and BehavePlus (Andrews 2014). Despite the wide operational use of the model, its performance has rarely been evaluated in the field, as gathering the required inputs can be quite difficult (Albini et al. 2012).

Although the NIROPS program has been collecting data on large fires in the USA for several years, there are few published studies that have directly utilized this data source. Several inherent limitations with the IR data have previously been identified (Zajkowski et al. 2003), but as far as the authors are aware, no attempt has been made to determine if the data are of suitable quality and quantity to evaluate spotting distances. In this study, we used the NIROPS data collected during the 2017 fire season in the Northern Rockies region of the USA to analyze the influence of several environment-, vegetation-, and fire-related variables on maximum spotting distance and to make comparisons with predictions from Albini's (1979) maximum spot fire distance model. We provide details about the methodology used, as well as the results from the statistical analysis. Information related to the limitations and issues encountered with using the NIROPS data are presented, in addition to their possible effects on assessing spotting distance.

Materials and methods

NIROPS data collection and preparation

All available NIROPS data captured during the 2017 fire season in the Northern Rockies region of the USA were downloaded from the National Interagency Fire Center (NIFC) FTP website and organized by fire name and date (available from https://ftp.nifc.gov/public/incident_specific_data/n_rockies/2017_fires/ [accessed 22 May 2018]). The available data represent those fires and dates that received a request for a flight, usually via the planning section associated with an incident management team, and were not omitted due to weather, technical issues, or availability. The IR flights were usually conducted between 1900 and 0500 local time, and the resulting images were processed by an IR interpreter and uploaded to the NIFC FTP site shortly thereafter. The IR interpreter's main role was to process the raw IR images to determine the boundary of the heat perimeters and the locations of hot spots and then configure the data and perimeter information into a format suitable for distribution to fire managers. The images were primarily gathered using the Phoenix Imaging System coupled with a dual-channel line scanner (3–5 μm and 8–14 μm bands) capable of detecting hot spots between 15 cm and 20 cm in diameter with an image resolution of 6.3 m per pixel at 3000 m above ground level (Greenfield et al. 2003). The processed data are available in several formats, but the ESRI shapefiles (*.shp) and the IR interpreter daily log were extracted for processing.

The NIROPS-produced shapefiles of interest in this study were isolated heat (points), intense heat (polygons), and associated heat perimeters (polygons). The intense heat polygons attempt to delineate areas of relatively high hot spot density, which are generally representative of active fire or recent fire activity. The heat perimeter polygons represent interpreted fire perimeters based on the captured heat signatures associated with the main fire, as well as the perimeter of smaller heat sources not connected to the main fire perimeter (Fig. 1). The heat perimeters are sometimes modified based on fire perimeter data captured in the field, usually with Global Positioning System devices, during the feedback process between the planning section of an incident management team and the IR interpreter.

Fig. 1. Location of the fire perimeter and spot fires for the Sheep Gap Fire located at the Lolo National Forest in Montana, USA, on 31 August 2017 at 2236 h local time.

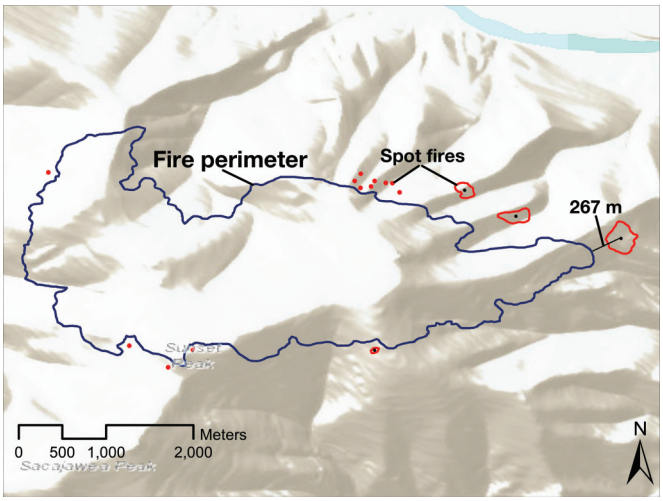

Spot fire identification and distance from the main fire perimeter were assessed by scripting an automated process in R using the geosphere, raster, rgdal, and sp packages (Pebesma and Bivand 2005; R Core Team 2015; Bivand et al. 2016; Hijmans 2016, 2017). Specifically, for each fire, the associated shapefiles were ordered by date and sequentially loaded to (*i*) identify spot fires, (*ii*) remove duplicate spot fires identified in previous time steps, (*iii*) calculate the size of the main fire area (m^2) and the perimeter-to-area ratio (m^{-1}, fire perimeter shape), (*iv*) calculate fire growth based on the percent increase in fire area since the previous time step, (*v*) calculate the proportion of the main fire area that contained intense heat, (*vi*) determine the size of each spot fire (m^2) and the geographic location of its centroid, and (*vii*) calculate the distance from each spot fire's centroid to the nearest main fire perimeter (m). As noted in the following Data analysis section, the available data were subset to include only data associated with consecutive day IR flights so that each spot fire's date of origin was known. The actual elapsed time between the IR flights varied according to the return times, which ranged from approximately 16 h to 30 h with a mean of 24 h. Spot fires were defined as polygons less than 10 ha in size that were not connected to the main fire perimeter and isolated heat sources (points) that fell outside of the main fire area. The 10 ha size threshold was arbitrarily selected based on an expectation that as spot fires grow larger, they become more likely to create additional spot fires (i.e., a spot from a spot), which could introduce a bias towards longer spotting distances. Sensitivity analysis of the calculated spotting distances to different size thresholds indicated the greatest sensitivity at sizes less than approximately 2–5 ha, which resulted in decreasing spotting distances. Thus, the 10 ha threshold was deemed a compromise to minimize biases towards either shorter or longer spotting distances.

Initial assessment of the data indicated that additional quality control would be needed to verify long-range spot fires. Spot fires that were >2.5 km from the main fire perimeter were verified by utilizing the IR interpreter's daily log and the fire perimeters in the days following their initial detection. In total, 48 long-range spot fire occurrences were evaluated and 38 were removed from the dataset, with approximately half of those removed described in the IR interpreter's daily log as being associated with campgrounds, railroad tracks, or warming fires. The remaining spot fires were not directly associated with a cause in the IR interpreter's daily log but were judged as unrealistic (e.g., >20 km) and failed to reappear as hot spots on the IR images in the following days.

Because of the low temporal resolution of the IR data, the time difference between a spot fire's detection by an IR flight and the spot fire's original creation could result in an underestimation of actual firebrand travel distance, as the main fire front likely continued to approach the spot fire before detection (see Results and discussion for more detail). To address this issue with the given data, a correction factor was added to the spot fire distances based on an estimate of the local average fire spread rate, the spot fire's size and shape at the time of detection, and a fixed ignition delay time. This correction factor was calculated for polygon-based spot fires (i.e., non-points) and then added to the initial spot fire distance to obtain the final spot fire distance that was used in the analysis.

The calculation of the correction factor for each spot fire that was a polygon comprised six primary steps. First, an average local fire spread rate (ROS_A, m·min^{-1}) was estimated by determining the distance that the main fire perimeter traveled in the vicinity of each spot fire during the 24 h period in which the spot fire originated (TD, m) and the time difference between return IR flights (TT, min; eq. 1).

$$(1) \qquad ROS_A = \frac{TD}{TT}$$

Second, the length-to-breadth ratio (LB) of each polygon was calculated by estimating the maximum length (ML, m) and maximum width (MW, m) of each polygon using the lakemorpho package in R (Hollister and Stachelek 2017; eq. 2).

$$(2) \qquad LB = \frac{ML}{MW}$$

The lakemorpho package estimates the ML of a polygon by finding the longest point-to-point distance between equally spaced points along the perimeter. The number of points along each perimeter was set to a minimum of 100 and increased by 25 points for every additional 0.4 ha increase in size. The MW was taken to be the line that intersected (and was perpendicular to) the line of ML. Third, the head fire-to-back fire spread ratio (HB; eq. 3) was calculated following Alexander (1985), which assumes that the fire's point of origin is the rear focus of an ellipse.

$$(3) \qquad HB = \frac{LB + (LB^2 - 1)^{0.5}}{LB - (LB^2 - 1)^{0.5}}$$

Fourth, head fire spread distance for each spot fire (HF, m) was estimated using HB and the ML of each polygon (eq. 4).

$$(4) \qquad HF = \frac{ML}{1 + (1/HB)}$$

Fifth, based on the assumption that the heading portion of the spot fire was moving at the same average rate as the main fire, which was probably not the case for the first 20–30 min (McAlpine and Wakimoto 1991), the time required to cover the head fire spread distance was calculated (HT, min; eq. 5).

$$(5) \qquad HT = \frac{HF}{ROS_A}$$

HT was then added to an estimated ignition delay (i.e., the time between when the firebrand landed and subsequent ignition and spread), which was set to a constant of 5 min following the range of values reported by Alexander and Cruz (2006), to obtain the total time after the firebrand landed, ignited the spot fire, and spread until detected by the IR flight (T, min). Sixth, the correction factor (CF, m) was calculated following eq. 6:

$$(6) \qquad CF = ROS_A(T)$$

Environmental data

To assess the influence of important environmental factors on spotting distance, additional data were collected (Table 1). Hourly wind speeds (m·s^{-1}) for the duration of each fire were estimated at 10 m height and 250 m resolution by using the Point Initialization feature and mass-conserving model within WindNinja (Forthofer et al. 2014). WindNinja simulates the effects of complex terrain on the wind field (including local changes in wind speed and direction) by minimizing the changes in the initial wind field while conserving mass. The Point Initialization feature integrates observations from local weather stations to help drive the simulation and force the output to match the observations (within 0.1 m·s^{-1}). The simulation domain was set to a 20 km × 20 km box centered on each fire, with all weather stations located within 5 km of the center and available via the MesoWest/SynopticLabs API (available from https://synopticlabs.org/api/mesonet/ [accessed 16 February 2018]) used for Point Initialization. The output raster grids were arranged according to the 24 h period (0000–2300 local time) in which the spot fires originated, and raster grids of the mean and maximum wind speed values at each cell location for each 24 h period within the domain were produced.

Vegetation-related data were retrieved from the LANDFIRE project for each fire (LF 1.4.0) (Rollins 2009). Specifically, raster grids of canopy cover (%), canopy height (m × 10), and biophysical setting were compiled and resampled to 250 m resolution within the Northern Rockies region. Biophysical setting was used to classify cells as belonging to specific cover type groups to facilitate the utilization of Albini's (1979) spot fire model; this is discussed in a following section, namely Albini (1979) spot fire model comparison. The primary tree species identified within the Northern Rockies region that corresponded to those available within Albini's (1979) model were Engelmann spruce (*Picea engelmannii* Parry ex Engelm.), lodgepole pine (*Pinus contorta* var. *latifolia* Engelm. ex S. Watson), Douglas-fir (*Pseudotsuga menziesii* (Mirb.) Franco), grand fir (*Abies grandis* (Douglas ex D. Don) Lindl.), and ponderosa pine (*Pinus ponderosa* Douglas ex P. Lawson & C. Lawson).

Terrain-related information, including slope position, elevation, and various metrics of terrain complexity, were compiled in 250 m raster grids for the Northern Rockies region. Specifically, slope position was calculated within a geographic information system (GIS) based on the topographic position index (Jenness 2006) and included six categories: Valley, Lower Slope, Flat Slope, Middle Slope, Upper Slope, and Ridge. For each fire perimeter, the mean and maximum elevations (m) that occurred within the main fire area were identified, as well as the standard deviation of elevation (m). For each spot fire, the distance from the lowest to highest elevation points (m) was identified within a circle having a 4 km radius centered at the spot fire location. The difference in elevation between the lowest and highest points (m) was also found within the same area.

Table 1. Variables analyzed to explain maximum spotting distance during the 2017 fire season in the Northern Rockies, USA.

Variable	Source	Description
Interpreted infrared data	National Interagency Fire Center (NIFC) FTP website	Geospatial infrared data (heat perimeters, intense heat polygons, and isolated heat points) captured approximately every 24 h for significant fires during the 2017 fire season in the Northern Rockies, USA
Main fire size (m^2)	R	Area within the main fire heat perimeter
Perimeter-to-area ratio (m^{-1})	R	Ratio of the total length of the main fire perimeter to the area within the main fire perimeter
Fire growth (%)	R	Percent increase in fire size compared to the previous approximately 24 h period
Proportion of main fire area as intense heat	R	Proportion of the main fire area that was classified as intense heat according to the infrared interpretation
10 m wind speed ($m \cdot s^{-1}$)	WindNinja (Forthofer et al. 2014)	Gridded hourly wind speeds in a 20 km × 20 km region surrounding each fire, estimated at 10 m height and 250 m resolution for the duration of each fire
24 h mean	R	Grids of the average 10 m wind speed at each grid cell for every 24 h period (0000–2300 local time) for the duration of each fire
24 h maximum	R	Grids of the maximum 10 m wind speed at each grid cell for every 24 h period (0000–2300 local time) for the duration of each fire
Vegetation		
Canopy cover (%)	LANDFIRE (Rollins 2009)	The percent cover of a forested canopy over the ground's surface, 250 m resolution
Canopy height (m × 10)	LANDFIRE (Rollins 2009)	The average height of the top of the vegetated canopy, 250 m resolution
Biophysical setting (283 levels)	LANDFIRE (Rollins 2009)	Vegetation type that may be dominant on the site, based on the current and historical disturbance regime, 250 m resolution
Terrain		
Elevation (m)	LANDFIRE (Rollins 2009)	The average, maximum, and standard deviation of elevation within the main fire area, based on a 250 m resolution digital elevation model
Slope position (six levels)	GIS (Jenness 2006)	Slope position based on the topographic position index (Jenness 2006): Valley, Lower Slope, Flat Slope, Middle Slope, Upper Slope, and Ridge
Ridge-to-valley elevation difference (m)	R	The difference between the highest and lowest elevation points within a 4 km radius centered at each spot fire location
Ridge-to-valley elevation distance (m)	R	The distance from the lowest to highest elevation points within a 4 km radius centered at each spot fire location

Note: GIS refers to a geographic information system, and R refers to the packages geosphere, raster, rgdal, and sp within the R computing environment (Pebesma and Bivand 2005; R Core Team 2015; Bivand et al. 2016; Hijmans 2016, 2017).

Data analysis

The environmental data were used to capture specific information related to the spot fire with the maximum distance for each unique combination of fire and day, referred to as a fire-day. For each fire-day, the geographic location of the spot fire with the maximum distance was identified, and the data (i.e., wind speed, slope position, vegetation, etc.) from the grid cell nearest to the spot fire along the main fire perimeter were extracted. Additionally, the mean, maximum (continuous variables), and mode (categorical variables) values for each variable were calculated for the grid cells located immediately adjacent to the nearest cell and for all grid cells located within the main fire area.

Prior to analysis, the dataset was modified to include only those fire-days that had a spot fire and spot fires for which the date of origin was known (i.e., the spot fires associated with the first day of each fire and spot fires associated with non-consecutive day IR flights were removed). Additionally, spot fires associated with fires where the mean canopy cover was less than 5% were removed to focus the analysis on spot fires originating from torching trees.

To investigate the effects of the environmental variables on maximum spotting distance, linear mixed-effects regression analysis was performed in R using the lme4 and lmerTest packages (Bates et al. 2015; Kuznetsova et al. 2017). Linear mixed-effects analysis evaluates the effects of the environmental variables of interest (fixed effects) while accounting for the random effects between subjects (i.e., the individual fires). Initial analysis of the maximum spotting distances among individual fires indicated substantial variability (Fig. 2) and thus confirmed the usefulness of the mixed-effects approach. The model parameters were estimated using maximum likelihood techniques, and the dependent variable (maximum spot fire distance) was transformed using the natural logarithm to address heteroscedasticity in the residuals. Fire was treated as a random effect (random y intercepts), whereas the environmental variables were treated as fixed effects. The environmental variables and relevant interactions were included in the model, and a backward selection process was used to remove non-significant (p value > 0.05) independent variables until a final model was obtained. The p values reported in this study

Fig. 2. Boxplots of the calculated maximum spot fire distances for the individual fires used in the analysis.

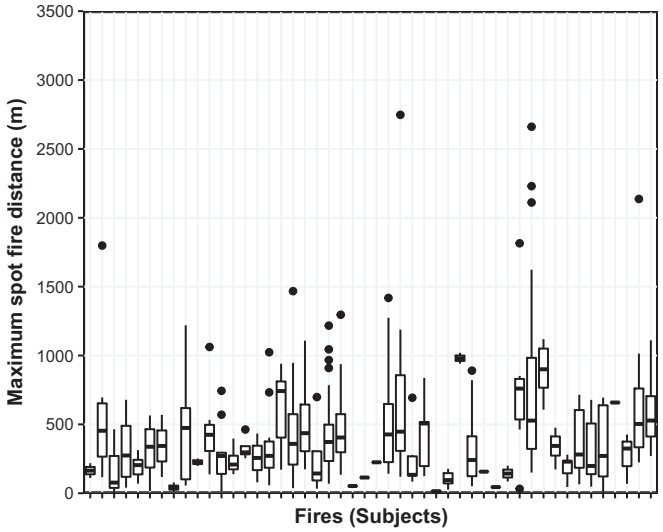

Table 2. Required inputs to run Albini's (1979) maximum spot fire distance model and the data source utilized for the present study.

Required input	Source
Downwind canopy height (m)	Assumed to equal the mean canopy height obtained from the grid cells nearest to the spot fire within the main fire perimeter
Torching tree height (m)	Set to be equivalent to the downwind canopy height
Spot tree species	Assigned based on the LANDFIRE Biophysical Setting classification for the grid cell nearest the spot fire within the main fire perimeter
Diameter at breast height (cm)	Estimated using the canopy height and height–diameter relationships published for the Inland Empire Variant of the Forest Vegetation Simulator for each tree species (Keyser 2015)
6.1 m wind speed ($m \cdot s^{-1}$)	The maximum 10 m wind speed recorded for the 24 h period during which the spot fire originated from all grid cells within the main fire area; transformed to the equivalent speed at 6.1 m height assuming a logarithmic wind profile and neutral atmospheric stability (Campbell and Norman 1998); two wind speed scenarios were evaluated based on whether the 24 h mean or maximum wind speed grids were utilized
Ridge-to-valley elevation difference (m)	Calculated as the difference in elevation between the highest and lowest elevation points within a circle having a 4 km radius centered at the spot fire location
Ridge-to-valley horizontal difference (m)	Calculated as the distance from the lowest to highest elevation points within a circle having a 4 km radius centered at the spot fire location
Spotting source location	The classified slope position (Jenness 2006) from the grid cell located nearest to the spot fire within the main fire perimeter; all "middle slope" classifications were assumed to be on the windward side of the slope
No. of torching trees	Varied from 1 to 10 trees

Table 3. Potential issues with using the National Infrared Operations (NIROPS) data to assess spotting distance.

Issue	Description	Possible effects
Data availability	NIROPS data are not consistently available for all fires and days	Missing data for smaller fires and inconsistent data for larger fires makes it difficult to determine when spot fires originated
Data quality	Heat sources that are unlikely to have originated from the fire are sometimes included; examples include isolated heat sources from train tracks and campfires from nearby campgrounds	Additional quality control is needed, which is aided by the use of the infrared interpreter daily log
	Inherent limitations with the infrared technology, including attenuation, heat source temperature (e.g., can only detect heat on the surface of targets), saturation, and the effects of cloud cover (Zajkowski et al. 2003; Allison et al. 2016)	Cloud and canopy cover sometimes obscure portions of fires, which potentially hide spot fires
	Raw data requires postprocessing by a qualified infrared interpreter	Unknown effects due to different interpretations of infrared images
Fire specific events	Difficult to determine the influence of fire suppression operations (e.g., firing operations) on spot fire distance	If firing operations away from the main fire do not join the main fire and (or) remain small by the time of the NIROPS flight, they may incorrectly be included as spot fires, potentially increasing the average spot fire distance
Spot fire origin (space and time)	The exact time and location of firebrand(s) produced are unknown; spot fire distance is calculated as the distance from the centroid to the nearest perimeter at the time of the flight	Underestimation of true spot fire distance as the main fire perimeter potentially has advanced closer to the spot fire by the time of the NIROPS flight; additionally, it is difficult to directly assess the effects of temporally varying weather (e.g., wind speed) on spot fire distance
Spot fire source	The type of fire behavior (e.g., crowning) and source (e.g., live tree, snag) that produced the firebrand(s) are unknown	Validation of existing spot fire models is difficult as many are based on knowing the source of the spot fire (e.g., crown fires, Albini et al. 2012; torching trees, Albini 1979)

have the same meaning as in other hypothesis testing, that is, the probability of rejecting the null hypothesis when it is true. The predictive power of the final model was assessed using the r.squaredGLMM function in the MuMIn package (Nakagawa and Schielzeth 2013), which employs methods to estimate the proportion of variance explained by the selected model using only the fixed effects (marginal R^2) and both the fixed and random effects (conditional R^2).

Albini (1979) spot fire model comparison

A comparison between the observed maximum spotting distance for each unique fire-day and the predicted theoretical maximum spot fire distance from Albini's (1979) model was completed. To obtain predictions from Albini's (1979) model, a command line version (available from https://github.com/firelab/behave [accessed 4 June 2018]) was used along with the inputs from the environmental variables previously described. Table 2 displays the required inputs for Albini's (1979) model and how the specific input values were obtained. Two wind speed scenarios were used based on whether the mean or maximum 24 h wind speed raster grids were utilized to extract the wind speed information. Additionally, the comparisons were made across a range of torching tree numbers, as it was not possible to gather or esti-

Fig. 3. Range of correction factors calculated to compensate for the the low temporal resolution of the infrared data (A). Distribution of spot fire distances for all spot fires assembled in the dataset (All) and for spot fires with the maximum distance for each unique fire-day combination (Maximum) (B).

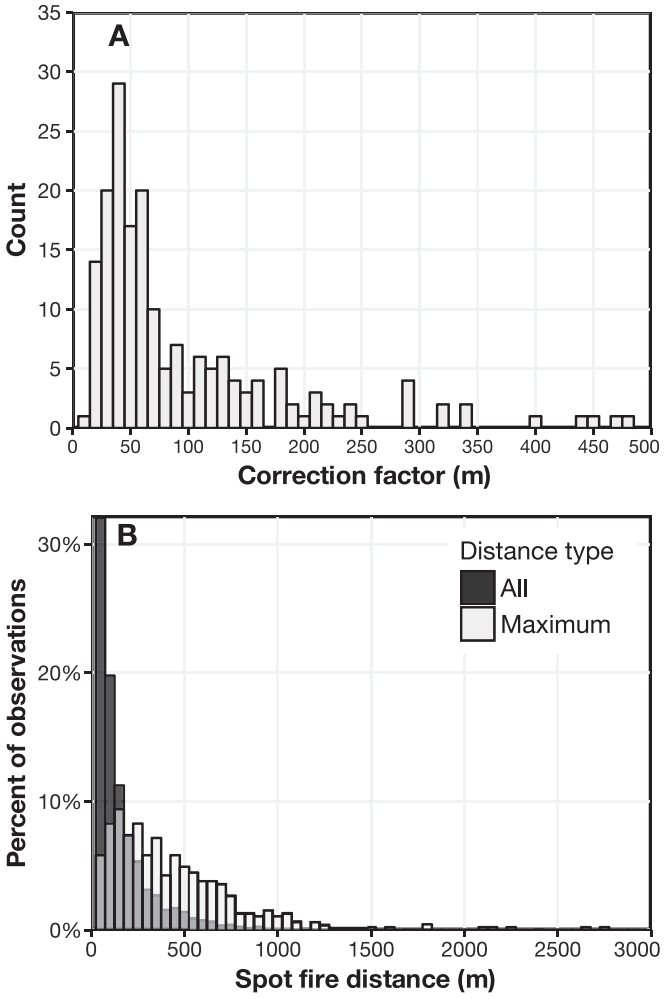

mate this value from our dataset. The raw errors (predicted theoretical maximum distance – observed maximum distance) were calculated for each fire-day and then grouped by each wind speed and torching tree scenario to evaluate model performance. The proportion of fire-days in which the raw errors were positive (i.e., an overprediction) was also calculated to assess performance.

Results and discussion

NIROPS data and spot fire distance

Estimating spotting distances using the NIROPS data required the understanding and mitigation of several potential issues (Table 3). The primary issue with the most potential to affect the broadscale results was related to the unknown time between when a spot fire occurred and when it was detected by the IR flight. If a spot fire occurred shortly before the flight, the distance from the centroid to the main fire perimeter was a relatively accurate representation of spotting distance; however, if a spot fire occurred well before the flight, the advance of the main fire front likely resulted in a calculated spotting distance that was shorter than the true distance. In an effort to address this issue, a correction factor was calculated and added to the spot fire distances based on an estimated local average fire spread rate, the size and shape of the spot fire, and a fixed ignition delay (Fig. 3A). The majority of spot fires were small, with mean and median sizes of 0.47 ha and 0.13 ha, respectively, which resulted in small correction factors that were mostly between 20 m and 80 m, although some exceeded 450 m. Analyses with and without the correction factor indicated that it had little influence on the results, which suggests that the effects of poor IR temporal resolution on spotting distance may be limited. Despite these results, it is important to acknowledge that the low temporal resolution of the NIROPS data is an inherent limitation of this data source and should be addressed in any future analyses.

Spot fire distance

The compiled dataset of spot fire distances contained 7214 unique spot fires that occurred on 48 fires over the course of 447 unique fire-day combinations. Approximately 94% of all spot fires had estimated distances that were ≤500 m, with a maximum verified distance of 2.7 km (Fig. 3B). The distribution of spot fire distances obtained in this study is similar (in terms of the shape and range of values) to other distributions produced using theoretical models (Wang 2011; Koo et al. 2012; Martin and Hillen 2016). In several simulation scenarios, both Wang (2011) and Koo et al. (2012) characterized the majority (>50%) of firebrands as landing less than 300–350 m from their source, depending on various modeling assumptions such as burnout time, firebrand shape, and initial mass. Profuse, short-range spotting (<500–800 m) has also been observed in other wildfires, especially those burning in Australian eucalypt stringybark forests, where long-distance spotting (i.e., >5 km) has been noted to require extended firebrand burnout times and extreme burning conditions (Cruz et al. 2012; Hall et al. 2015).

It is worth noting that such short-range spotting distances imply that the main fire front was moving slowly at the time the spot fires were detected. Alexander and Cruz (2006) reported that for spread rates greater than approximately 20 m·min^{-1}, spotting distances in excess of 300 m are needed for newly ignited spot fires to contribute to forward spread and avoid being overtaken by the main flame front. As the majority of spot fires detected with the NIROPS data were less than 500 m from the main fire perimeter, it is probable that the main fire front was moving slowly at the time of the IR flight, as a fast-moving fire front would have likely overtaken most of the spot fires before they could have been detected. The estimates of the local average fire spread rate that were compiled to calculate the correction factors confirmed that the spread rates were generally low (i.e., <1 m·min^{-1}) but did approach 12 m·min^{-1} for some fires.

The maximum spotting distances for each unique fire-day had mean and median values of 436 m and 355 m, respectively. Additionally, there were 31 unique fire-days in which the maximum recorded distance exceeded 1 km. The farthest verified distance of 2.7 km occurred sometime on 6 September during the Monahan Fire in the Flathead National Forest in northwestern Montana. These maximum distances are similar to distances observed on other large fires that have occurred in the Northern Rocky Mountains, including a 2–3 km distance witnessed on 8 August 1936 during the Galatea fire in the Canadian Rockies (Fryer and Johnson 1988), a ~1 km distance between 29 and 30 August 1967 during the Sundance Fire in northern Idaho (Anderson 1968), and a 1–2 km distance during the 2003 fire season in British Columbia (Beck and Simpson 2007). However, in this dataset, we did not record the extreme distances that have also been observed such as the 16–19 km distances seen during a 26 km fire run over 9 h on 1 September 1967 during the Sundance Fire (Anderson 1968).

The linear mixed-effects analysis of maximum spotting distance produced a model that identified several significant relationships with the environment-, vegetation-, and fire-related variables and explained approximately 13% and 38% of the total variability based on the fixed effects alone and both the fixed and random effects, respectively (Table 4). A significant positive correlation was identified between the maximum spot fire distance and

Table 4. Fixed-effects parameter estimates resulting from the mixed-effects regression analysis of the natural logarithm of maximum spot fire distance (dependent variable) against several environmental variables.

Parameter	Coefficient	SE	Standardized coefficient	Degrees of freedom	*t* value	*p* value (>|*t*|)
Intercept	7.4202	0.4133	—	78	17.95	<0.001
Ridge-to-valley elevation difference (m)	−0.0011	0.0002	−0.24	313	−4.31	<0.001
Canopy height (m × 10)	−0.0038	0.0019	−0.15	52	−2.02	0.049
Perimeter-to-area ratio (m^{-1})	−81.1301	29.8116	−0.16	195	−2.72	0.007
Fire growth (%)	0.0069	0.0048	0.18	447	1.43	0.154
Mean 10 m wind speed ($m \cdot s^{-1}$)	−0.0377	0.0259	−0.04	411	−1.46	0.146
Fire growth × wind speed	0.002	0.001	0.07	446	2.03	0.043

Note: Standard errors (SE) are reported along with the Satterthwaite approximations for degrees of freedom.

an interaction between the maximum 10 m wind speed recorded within the main fire perimeter using the mean 24 h wind speed grid and fire growth. According to the proposed statistical model, fires that grew substantially compared with the previous day (>50% increase in growth) and had relatively high wind speeds (>10 $m \cdot s^{-1}$) had the potential to produce spot fire distances in excess of 1 km (Fig. 4A). The importance of wind speed on potential spotting distance is well known (Albini 1983; Pastor et al. 2003), but the dependence on fire growth suggests that wind and other conditions associated with large fire growth (e.g., convection column development) are needed for long-range spotting to occur. This finding is in line with several theoretical (Lee and Hellman 1970; Albini 1979; Woycheese et al. 1999; Albini et al. 2012) and experimental (Tohidi and Kaye 2017) analyses that emphasize the importance of characteristics of the convection column, heat release rate, or lofting height in their estimation of potential spotting distance.

Three variables in the mixed-effects model analysis had negative correlations with maximum spot fire distance: the difference in elevation between the highest and lowest points within a 4 km radius circle centered at the spot fire, mean canopy height within the fire area, and the perimeter-to-area ratio of the main fire. As the difference in elevation between the highest and lowest elevation points decreased (i.e., the terrain became flatter), the maximum spot fire distance increased (Fig. 4B). This terrain effect is similar to the one proposed by Albini (1979) for torching trees, in which steep elevation gradients in complex terrain decrease potential spotting distance when spot fires originate in a valley bottom or on the leeward side of slopes. The proposed model also suggested that as the perimeter-to-area ratio decreased (i.e., the fires become more elliptical), the maximum spot fire distance increased. Eccentricity in fire shape is associated with an increase in effective wind speed, where the combined influence of wind and slope increases the length-to-width ratio of fires, which is a result of fast-spreading, higher intensity fires that facilitate long-range spotting (Anderson 1983; Alexander 1985).

Comparison with Albini's (1979) model

The comparisons of the observed maximum spotting distances with the predictions from Albini's (1979) model indicated that the proportion of fire-days with an overprediction (i.e., raw error > 0) varied primarily according to the wind speed scenario used to run the model (Fig. 5). When the 24 h mean wind speed grids were utilized, Albini's (1979) model had a tendency to produce maximum spotting distances that were less than observed, with fewer than 45% of the fire-days having an overprediction, which resulted in a mean underprediction of approximately 186 m across the range of torching tree numbers considered (Fig. 5A). However, when the 24 h maximum wind speeds grids were utilized, the majority of fire-days had an overprediction, the mean of which was approximately 149 m (Fig. 5B). Given the unknowns in regards to the static and dynamic factors (both local and broadscale) that influence spotting distance, it is difficult to determine the reasons for the observed underpredictions produced by Albini's (1979) model. Low-quality and inappropriate inputs such as inaccurate wind speed information or the failure of Albini's (1979) model to incorporate additional important factors may have led to some of the underprediction bias. The results of this analysis suggest that, in terms of operational application, it is important to utilize the

Fig. 4. Predicted maximum spot fire distance across increasing fire growth and mean 10 m wind speed (A) and increasing fire growth and ridge-to-valley elevation distance (B). The model predictions are based on the results from the linear mixed-effects analysis using mean values for the other significant predictor variables gathered from a random fire in the dataset. Note the change in axis direction for the ridge-to-valley elevation difference and mean 10 m wind speed variables.

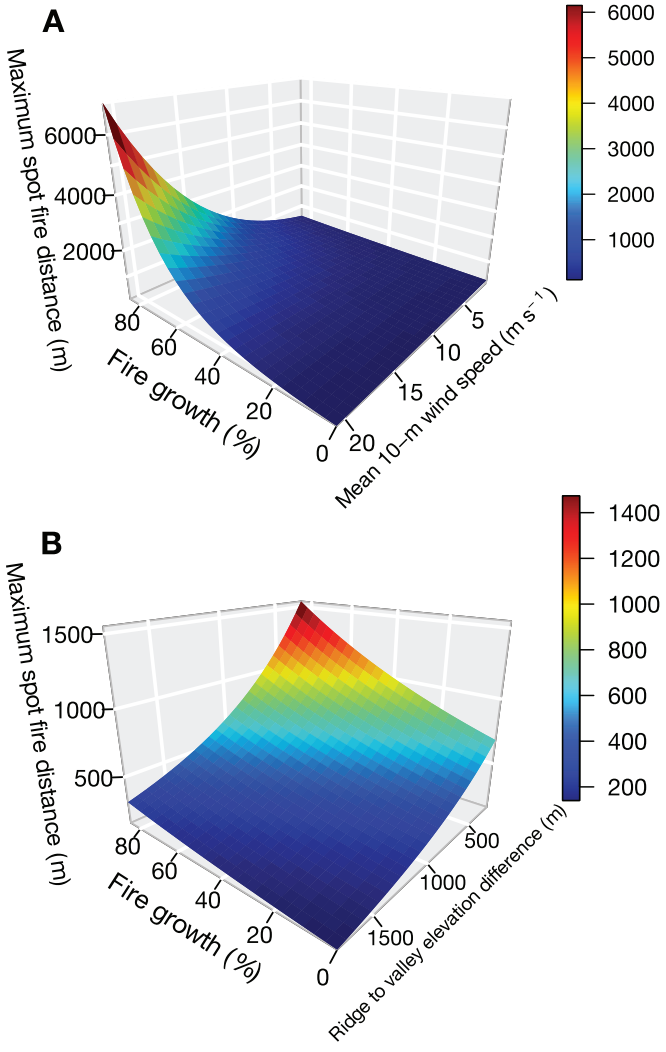

Fig. 5. Boxplots of the raw error (Albini's (1979) model prediction – observed maximum spot fire distance) for each unique fire-day across an increasing number of torching trees based on using the 24 h mean wind speed values (A) and the 24 h maximum wind speed values (B).

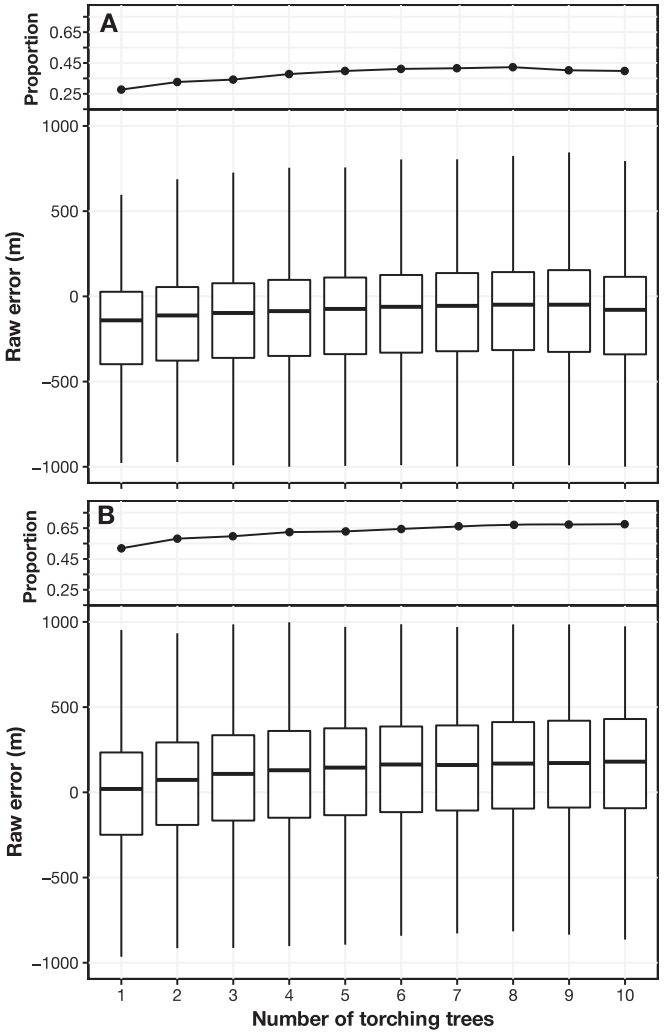

high end of wind speed forecasts or model simulation results when making predictions with Albini's (1979) model. This will increase the likelihood that Albini's (1979) model provides an overestimate of maximum spotting distance, which, in terms of operational application, is more desirable than an underestimate.

Although rare, previous comparisons of predictions from Albini's (1979) model against actual observations suggest that it usually overpredicts maximum spot fire distance (Albini et al. 2012). During the 1980 Mack Lake Fire in Michigan, Simard et al. (1983) found that predictions were in good agreement with observations, with a predicted distance of 0.54 km compared with an observed distance of 0.40 km. Likewise, Rothermel (1983) reported that for two cases on the Lily Lake Fire in Utah, the predicted low, medium, and high estimates exceeded the actual spotting distance for one case, and the predicted high estimate exceeded the actual distance for another case.

Summary and conclusions

An analysis of the broadscale and temporally limited data collected by the NIROPS program during the 2017 fire season in the Northern Rockies region of the USA was completed. The results revealed that the majority of spotting distances were ≤500 m and that medium-range spotting (1–3 km) was somewhat rare, being observed on only 31 of 447 possible unique fire-days. The analysis also identified several environmental variables that were related to maximum spotting distance, including the ridge-to-valley elevation difference around the spot fire, fire perimeter shape, canopy height, and an interaction between fire growth and wind speed. A particularly important finding was that a combination of high wind speeds and substantial fire growth increased the likelihood of observing spotting distances in excess of 1 km. Comparisons of the dataset with predictions from a popular model developed to identify the theoretical upper limit of spotting distance indicated that fire behavior modelers should use the high end of wind speed forecasts or wind model simulation results to help ensure that the predictions are conservative and overestimate potential spotting distance.

Although the analysis of spotting distances with the NIROPS data indicated that there were several significant statistical relationships that were corroborated by previous findings from theoretical, experimental, and empirical observations, it is important to acknowledge the limitations with this data source. We found that manual quality control procedures were needed to verify long-distance spot fires and a methodology was needed to address a known bias produced by the time difference between when a spot fire is initially created and when it is detected by an IR flight. Despite these limitations, it appears that the data produced by the NIROPS program may be a resource to consider utilizing in future research.

Acknowledgements

This work was supported by the Joint Fire Science Program through Project 15-1-04-9, the National Fire Plan through the Washington Office of the Forest Service Deputy Chief for Research, and the Wildland Fire Management Research Development & Application Program. We gratefully acknowledge review of the manuscript by M.E. Alexander, the Associate Editor, and two anonymous reviewers.

References

Albini, F.A. 1979. Spot fire distance from burning trees — a predictive model [online]. USDA For. Serv. Gen. Tech. Rep. INT-56. Available from https://www.frames.gov/documents/behaveplus/publications/Albini_1979_INT-GTR-056_ocr.pdf [accessed 12 February 2018].

Albini, F.A. 1983. Potential spotting distance from wind-driven surface fires [online]. USDA For. Serv. Res. Pap. INT-309. Available from https://sagemap.wr.usgs.gov/Docs/Albini.1983.RP-INT-309.pdf [accessed 12 February 2018].

Albini, F.A., Alexander, M.E., and Cruz, M.G. 2012. A mathematical model for predicting the maximum potential spotting distance from a crown fire. Int. J. Wildland Fire, **21**(5): 609–627. doi:10.1071/WF11020.

Alexander, M.E. 1985. Estimating the length-to-breadth ratio of elliptical forest fire patterns [online]. *In* Proceedings of the Eighth Conference on Fire and Forest Meteorology, Detroit, Mich., 29 April – 2 May 1985. *Edited by* L.R. Donoghue and R.E. Martin. Society of American Foresters, Bethesda, Md. SAF Publication 85-04. Available from http://cfs.nrcan.gc.ca/pubwarehouse/pdfs/11401.pdf [accessed 5 March 2018].

Alexander, M.E. 2000. Fire behaviour as a factor in forest and rural fire suppression [online]. Forest research in association with New Zealand Fire Service Commission and National Rural Fire Authority, For. Res. Bull. 197, Forest and Rural Fire Science and Technology Series Report 5. Available from http://cfs.nrcan.gc.ca/pubwarehouse/pdfs/18242.pdf [accessed 12 February 2018].

Alexander, M.E., and Cruz, M.G. 2006. Evaluating a model for predicting active crown fire rate of spread using wildfire observations. Can. J. For. Res. **36**(11): 3015–3028. doi:10.1139/x06-174.

Allison, R.S., Johnston, J.M., Craig, G., and Jennings, S. 2016. Airborne optical and thermal remote sensing for wildfire detection and monitoring. Sensors, **16**(8): 1310. doi:10.3390/s16081310.

Anderson, H.E. 1968. Sundance Fire: an analysis of fire phenomena [online]. USDA For. Serv. Res. Pap. INT-56. Available from https://www.fs.fed.us/rm/pubs_int/int_rp056.pdf [accessed 12 February 2018].

Anderson, H.E. 1983. Predicting wind-driven wild land fire size and shape [online]. USDA For. Serv. Res. Pap. INT-305. Available from https://archive.org/details/predictingwinddr305ande [accessed 12 February 2018].

Andrews, P.L. 2014. Current status and future needs of the BehavePlus Fire Modeling System. Int. J. Wildland Fire, **23**(1): 21. doi:10.1071/WF12167.

Bates, D., Maechler, M., Bolker, B., and Walker, S. 2015. Fitting linear mixed-effects models using lme4. J. Stat. Softw. **67**(1): 1–48. doi:10.18637/jss.v067.i01.

Beck, J., and Simpson, B. 2007. Wildfire threat analysis and the development of a fuel management strategy for British Columbia. *In* Proceedings of Wildfire 2007 — 4th International Wildland Fire Conference, Seville, Spain, 13–17 May 2007. Ministry of Environment and Junta de Andalucia, Seville, Spain. pp. 1–12.

Bivand, R., Keitt, T., and Rowlingson, B. 2016. rgdal: bindings for the geospatial data abstraction library [online]. R package version 1.2-5. Available from https://CRAN.R-project.org/package=rgdal [accessed 24 May 2018].

Campbell, G.S., and Norman, J.M. (*Editors*). 1998. Wind. *In* An introduction to environmental biophysics. Springer, New York. pp. 63–75. doi:10.1007/978-1-4612-1626-1_5.

Cruz, M.G., Sullivan, A.L., Gould, J.S., Sims, N.C., Bannister, A.J., Hollis, J.J., and Hurley, R.J. 2012. Anatomy of a catastrophic wildfire: the Black Saturday Kilmore East fire in Victoria, Australia. For. Ecol. Manage. **284**: 269–285. doi:10.1016/j.foreco.2012.02.035.

Finney, M.A. 2004. FARSITE: Fire area simulator — model development and evaluation [online]. USDA For. Serv. Res. Pap. RMRS-4. Revised. Available from https://www.fs.fed.us/rm/pubs/rmrs_rp004.pdf [accessed 12 February 2018].

Forthofer, J.M., Butler, B.W., and Wagenbrenner, N.S. 2014. A comparison of three approaches for simulating fine-scale surface winds in support of wildland fire management. Part I. Model formulation and comparison against measurements. Int. J. Wildland Fire, **23**(7): 969–981. doi:10.1071/WF12089.

Fryer, G.I., and Johnson, E.A. 1988. Reconstructing fire behaviour and effects in a subalpine forest. J. Appl. Ecol. **25**(3): 1063–1072. doi:10.2307/2403766.

Greenfield, P.H., Smith, W., and Chamberlain, D.C. 2003. Phoenix — the new Forest Service airborne infrared fire detection and mapping system [online]. *In* 2nd International Wildland Fire Ecology and Management Congress and 5th Symposium on Fire and Forest Meteorology, Orlando, Fla., 16–20 November 2003. American Meteorological Society. p. J1G.3. Available from https://ams.confex.com/ams/FIRE2003/techprogram/paper_66675.htm [accessed 12 February 2018].

Hall, J., Ellis, P.F., Cary, G.J., Bishop, G., and Sullivan, A.L. 2015. Long-distance spotting potential of bark strips of a ribbon gum (*Eucalyptus viminalis*). Int. J. Wildland Fire, **24**(8): 1109–1117. doi:10.1071/WF15031.

Hijmans, R.J. 2016. geosphere: spherical trigonometry [online]. R package version 1.5-5. Available from https://CRAN.R-project.org/package=geosphere [accessed 24 May 2018].

Hijmans, R.J. 2017. raster: geographic data analysis and modeling [online]. R package version 2.6-7. Available from https://CRAN.R-project.org/package=raster [accessed 24 May 2018].

Hollister, J., and Stachelek, J. 2017. lakemorpho: calculating lake morphometry metrics in R. F1000Research, **6**: 1718. doi:10.12688/f1000research.12512.1. PMID:29188019.

Jenness, J. 2006. Topographic Position Index (tpi_jen.avx) extension for ArcView 3.x [online]. Jenness Enterprises. Available from http://www.jennessent.com/arcview/tpi.htm [accessed 7 February 2017].

Keyser, C.E. 2015. Inland Empire (IE) variant overview — Forest Vegetation Simulator [online]. USDA For. Serv. Internal Rep. Available from https://www.fs.fed.us/fmsc/ftp/fvs/docs/overviews/FVSie_Overview.pdf [accessed 12 February 2018].

Koo, E., Linn, R.R., Pagni, P.J., and Edminster, C.B. 2012. Modelling firebrand transport in wildfires using HIGRAD/FIRETEC. Int. J. Wildland Fire, **21**(4): 396–417. doi:10.1071/WF09146.

Kuznetsova, A., Brockhoff, P.B., and Christensen, R.H.B. 2017. lmerTest package: tests in linear mixed effects models. J. Stat. Softw. **82**(13): 1–26. doi:10.18637/jss.v082.i13.

Lee, S.-L., and Hellman, J.M. 1970. Firebrand trajectory study using an empirical velocity-dependent burning law. Combust. Flame, **15**(3): 265–274. doi:10.1016/0010-2180(70)90006-4.

Martin, J., and Hillen, T. 2016. The spotting distribution of wildfires. Appl. Sci. **6**(6): 177. doi:10.3390/app6060177.

McAlpine, R.S., and Wakimoto, R.H. 1991. The acceleration of fire from point source to equilibrium spread. For. Sci. **37**: 1314–1337.

Nakagawa, S., and Schielzeth, H. 2013. A general and simple method for obtaining R^2 from generalized linear mixed-effects models. Methods Ecol. Evol. **4**(2): 133–142. doi:10.1111/j.2041-210x.2012.00261.x.

National Interagency Coordination Center (NICC). 2017. National Interagency Coordination Center wildland fire summary and statistics annual report [online]. Boise, Idaho. Available from https://www.predictiveservices.nifc.gov/intelligence/2017_statssumm/annual_report_2017.pdf [accessed 12 February 2018].

National Interagency Fire Center (NIFC). 2017. Northern Rockies Geographic Area fire season assessment 2017 [online]. Boise, Idaho. Available from http://dnrc.mt.gov/news/NorthernRockiesGeographicArea852017.pdf [accessed 28 January 2019].

Noonan-Wright, E.K., Opperman, T.S., Finney, M.A., Zimmerman, G.T., Seli, R.C., Elenz, L.M., Calkin, D.E., and Fiedler, J.R. 2011. Developing the US Wildland Fire Decision Support System. J. Combust. **2011**: 168473. doi:10.1155/2011/168473.

Pastor, E., Zárate, L., Planas, E., and Arnaldos, J. 2003. Mathematical models and calculation systems for the study of wildland fire behaviour. Prog. Energy Combust. Sci. **29**(2): 139–153. doi:10.1016/S0360-1285(03)00017-0.

Pebesma, E.J., and Bivand, R.S. 2005. Classes and methods for spatial data in R. R News, **5**(2): 9–13.

R Core Team. 2015. R: a language and environment for statistical computing [online]. R Foundation for Statistical Computing, Vienna, Austria. Available from https://www.r-project.org/ [accessed 12 February 2018].

Rollins, M.G. 2009. LANDFIRE: a nationally consistent vegetation, wildland fire, and fuel assessment. Int. J. Wildland Fire, **18**(3): 235–249. doi:10.1071/WF08088.

Rothermel, R.C. 1983. How to predict the spread and intensity of forest and range fires. USDA For. Serv. Gen. Tech. Rep. INT-143. doi:10.2737/INT-GTR-143.

Simard, A.J., Haines, D.A., Blank, R.W., and Frost, J.S. 1983. The Mack Lake fire [online]. USDA For. Serv. Gen. Tech. Rep. NC-83. Available from https://www.nrs.fs.fed.us/pubs/gtr/gtr_nc083.pdf [accessed 12 February 2018].

Tohidi, A., and Kaye, N.B. 2017. Comprehensive wind tunnel experiments of lofting and downwind transport of non-combusting rod-like model firebrands during firebrand shower scenarios. Fire Saf. J. **90**: 95–111. doi:10.1016/j.firesaf.2017.04.032.

Wang, H.-H. 2011. Analysis on downwind distribution of firebrands sourced from a wildland fire. Fire Technol. **47**(2): 321–340. doi:10.1007/s10694-009-0134-4.

Woycheese, J.P., Pagni, P.J., and Liepmann, D. 1999. Brand propagation from large-scale fires. J. Fire Prot. Eng. **10**(2): 32–44. doi:10.1177/104239159901000203.

Zajkowski, T.J., Queen, L.P., and VanBuren, D. 2003. Infrared users' guide and vendor listings [online]. USDA For. Serv. Remote Sensing Applications Center RSAC-1309-RPT1. Available from http://www.dmphotonics.com/Infrared%20Fire%20Imaging/Infrared%20Field%20Users%20Guide%20and%20Vendor%20Listings%2008-1309-RPT1.pdf [accessed 12 February 2018].